Universiteit
Leiden
The Netherlands

Kiloparsec-scale alignment of a radio jet with cool gas and dust in a z ~ 6 quasar

Walter, F.; Bañados, E.; Carilli, C.; Neeleman, M.; Connor, T.; Decarli, R.; ... ; Venemans, B.P.

Citation
Walter, F., Bañados, E., Carilli, C., Neeleman, M., Connor, T., Decarli, R., ... Venemans, B. P. (2025). Kiloparsec-scale alignment of a radio jet with cool gas and dust in a z ~ 6 quasar. *Astrophysical Journal Letters*, *983*(1). doi:10.3847/2041-8213/adc2f5

Version:	Publisher's Version
License:	Creative Commons CC BY 4.0 license
Downloaded from:	https://hdl.handle.net/1887/4289858

Note: To cite this publication please use the final published version (if applicable).

The Astrophysical Journal Letters, 983:L8 (7pp), 2025 April 10 https://doi.org/10.3847/2041-8213/adc2f5
© 2025. The Author(s). Published by the American Astronomical Society.
OPEN ACCESS

Kiloparsec-scale Alignment of a Radio Jet with Cool Gas and Dust in a $z \sim 6$ Quasar

Fabian Walter[1,2,3], Eduardo Bañados[1], Chris Carilli[3], Marcel Neeleman[4], Thomas Connor[5], Roberto Decarli[6], Emanuele Paulo Farina[7], Yana Khusanova[1], Chiara Mazzucchelli[8], Romain Meyer[1,9], Emmanuel Momjian[3], Hans–Walter Rix[1], Sofía Rojas-Ruiz[10], and Bram Venemans[11]
[1] Max Planck Institut für Astronomie, Königstuhl 17, D-69117 Heidelberg, Germany; walter@mpia.de
[2] California Institute of Technology, Pasadena, CA 91125, USA
[3] National Radio Astronomy Observatory, Pete V. Domenici Array Science Center, P.O. Box O, Socorro, NM 87801, USA
[4] National Radio Astronomy Observatory, 520 Edgemont Road, Charlottesville, VA 22903, USA
[5] Center for Astrophysics | Harvard & Smithsonian, 60 Garden St., Cambridge, MA 02138, USA
[6] INAF-Osservatorio di Astrofisica e Scienza dello Spazio, via Gobetti 93/3, I-40129, Bologna, Italy
[7] GEMINI Observatory Northern Operations Center, 670 N. A'ohoku Place - Hilo, HI 96720, USA
[8] Instituto de Estudios Astrofísicos, Facultad de Ingeniería y Ciencias, Universidad Diego Portales, Avenida Ejercito Libertador 441, Santiago, Chile
[9] Department of Astronomy, University of Geneva, Chemin Pegasi 51, 1290 Versoix, Switzerland
[10] Department of Physics and Astronomy, University of California, Los Angeles, 430 Portola Plaza, Los Angeles, CA 90095, USA
[11] Leiden Observatory, Leiden University, PO Box 9513, 2300 RA Leiden, The Netherlands
Received 2025 January 29; revised 2025 March 16; accepted 2025 March 17; published 2025 April 4

Abstract

We present high-angular-resolution (0.″068, ∼400 pc) Atacama Large Millimeter/submillimeter Array (ALMA) imaging of the [C II] line and dust continuum emission of PSO J352.4034–15.3373, a radio-loud quasar at $z = 5.83$. The observations reveal a remarkably close match between the orientation of the [C II] and thermal dust emission mapped by ALMA and radio synchrotron emission of a radio jet previously mapped by the Very Long Baseline Array. This narrow alignment extends over ∼4 kpc, reminiscent of the well-studied "alignment effect" in lower-redshift radio galaxies. The [C II] kinematics show a linear increase in velocity with galactocentric radii up to ∼200 km s^{-1} at $r = 2$ kpc, consistent with bulk motions within the galaxy potential, and not relativistic jet motions. The kinematics and respective morphologies are consistent with a picture in which the relativistic jet injects energy into the interstellar medium (potentially leading to subsequent star formation), giving rise to the observed alignment and significant ($\gtrsim$100 km s^{-1}) [C II] velocity dispersion within the host galaxy on kiloparsec scales. Indeed, the astonishingly close alignment and narrow linearity of the radio jet with the [C II] and dust emission are hard to conceive without some fundamental relationship between the two.

Unified Astronomy Thesaurus concepts: Quasars (1319); Reionization (1383); Interstellar medium (847)

1. Introduction

Ever since their first detection more than 20 yr ago (X. Fan et al. 2001), the existence of quasars at Cosmic Dawn ($z \gtrsim 6$; i.e., when the Universe was <1 Gyr old) has challenged our understanding of early supermassive black hole (SMBH) and galaxy formation (e.g., review by X. Fan et al. 2023). Their high rest-frame UV brightness and broad-line region properties provide clear evidence that the centers of these quasars are powered by accreting SMBHs that often exceed masses of $10^9\,M_\odot$. These SMBHs thus must have accreted copious amounts of mass throughout their short lifetimes. To explain this rapid growth, theories invariably predict that quasars emerge in overdense environments through rapid gas accretion and mergers. These processes also build up the host galaxies, but theories disagree if the growth of the black holes outpaces the growth of the galaxies or vice versa (e.g., M. Habouzit et al. 2021; M. Volonteri et al. 2021).

One of the early puzzling findings from the pre–Atacama Large Millimeter/submillimeter Array (ALMA) era was the detection of large amounts of cold dust and molecular gas in the host galaxy of the $z = 6.4$ quasar J1148+5251 (exceeding gas masses of $10^{10}\,M_\odot$; F. Walter et al. 2003, 2004; F. Bertoldi et al. 2003; R. Maiolino et al. 2005), demonstrating the presence of highly enriched gas on kiloparsec scales within the first gigayear of the Universe. Today, out of the ∼300 quasars that are known at redshifts $z \gtrsim 6$, about 100 have been observed with ALMA, and most are detected through the redshifted 158 μm line of ionized carbon ([C II]) and the underlying thermal dust continuum (e.g., R. Decarli et al. 2018; B. P. Venemans et al. 2018; X. Fan et al. 2023). This interstellar medium (traced through dust continuum, [C II], and CO emission lines) is found to be in a cold phase (∼50 K; e.g., C. Leipski et al. 2014) and is thought to be heated by star formation in the quasar hosts. With the advent of JWST, star formation and stellar mass tracers are now also being routinely detected in this high-redshift quasar population (e.g., X. Ding et al. 2023; R. Decarli et al. 2024; M. Onoue et al. 2024).

So far, high-spatial-resolution (few–100 pc) ALMA imaging of the dust and [C II] in $z \gtrsim 6$ quasar host galaxies have found little evidence for interactions or feedback between the central SMBH and the host galaxy (B. P. Venemans et al. 2019; F. Walter et al. 2022; R. A. Meyer et al. 2023; M. Neeleman et al. 2023; R. A. Meyer et al. 2025). This is surprising, as the active galactic nucleus (AGN) or quasar phase of a galaxy, i.e., when the central SMBH is actively accreting material and releasing energy into the surrounding medium, is thought to play an important role in shaping its host galaxy, thus affecting the process of galaxy evolution (e.g., A. C. Fabian 2012; D. Wylezalek & R. Morganti 2018). For example, relativistic

Original content from this work may be used under the terms of the Creative Commons Attribution 4.0 licence. Any further distribution of this work must maintain attribution to the author(s) and the title of the work, journal citation and DOI.

jets powered by SMBHs are thought to affect their environment on galactic (kiloparsec or even 10 s of kiloparsec) scales (the so-called kinetic or radio-mode feedback). This kinetic feedback is often associated with low-power AGN, but this mode can also be significant on sources with high accretion rates, such as quasars (e.g., H. R. Russell et al. 2013; N. P. H. Nesvadba et al. 2017).

In this Letter, we present high-resolution ALMA observations to map the dust and [C II] gas of the $z = 5.83$ quasar PSO J352.4034−15.3373 (hereafter P352–15; E. Bañados et al. 2018). This quasar was originally selected through standard color-selection techniques and later identified to be one of the few radio-loud quasars known at the time at $z \sim 6$. Very Long Baseline Array (VLBA) observations at high resolution ($\sim 0\farcs017$, $\sim$100 pc) revealed that P352–15 hosts the largest jet observed in the Universe's first billion years (E. Momjian et al. 2018), with X-ray observations showing that the jet may extend as much as 50 kpc (T. Connor et al. 2021). Follow-up low (kiloparsec-scale)-resolution ALMA [C II] and dust continuum mapping of P352–15 revealed typical gas and dust masses as compared to the $z \sim 6$ quasar population: indeed, P352–15 broadly follows the $L_{\rm FIR}$—$L_{\rm [CII]}$ distribution found in the $z \sim 6$–7 quasar distribution. The far-infrared (FIR)–radio spectral energy distribution implies that the ALMA continuum emission is not significantly affected (at most at a 10% level) by the synchrotron emission seen in the radio regime (S. Rojas-Ruiz et al. 2021).

We use a flat cosmology with $H_0 = 70\,{\rm km\,s^{-1}\,Mpc^{-1}}$, $\Omega_M = 0.3$, and $\Omega_\Lambda = 0.7$. At $z = 5.831$, the Universe is 950 Myr old, and one proper kiloparsec corresponds to $0\farcs172$ ($1''$ equals 5.81 kpc).

2. Observations

P352–15 was observed in ALMA Band 7 (S. Mahieu et al. 2012) to map its (rest-frame) 158 μm [C II] emission line and underlying continuum emission. The observations were carried out during two different ALMA Cycles (cycles 6 and 9) with similar antenna configurations (5th [80th] percentiles of 336 m [3626 m] and 315 m [3282 m], respectively). The first set of observations was conducted in Cycle 6 on UT 2019 July 31 (ALMA PID 2018.1.00656.S) for a total duration of 1.7 hr (49 minutes on source). The second set of observations was conducted in Cycle 9 between UT 2023 June 22 and June 2023 June 30 (ALMA PID 2022.1.01587.S) with a total time of 29.8 hr (12.9 hr on source). The blazar J0006−0623 was used as a flux density scale and bandpass calibrator, and the blazar J2331−1556 was used as a phase calibrator. One of the 1.875 GHz spectral windows was centered on the expected frequency of the redshifted [C II] emission (277.8 GHz), whereas the remaining 1.875 GHz spectral windows were set up to detect continuum emission at sky frequencies of 279.8, 289.9, and 291.9 GHz.

The data from 2018.1.00656.S and 2022.1.01587.S were processed using the Cycle-specific ALMA pipelines (T. R. Hunter et al. 2023), which are part of the Common Astronomy Software Application (CASA) package (V.5.6.1-8 and V6.2.1-7 for Cycle 6 and Cycle 9, respectively; J. P. McMullin et al. 2007; CASA Team et al. 2022). The two data sets were then combined using the task concat in the most recent version of CASA at the time of analysis (V6.5.2-26). Further imaging and processing were done in this version of CASA as well.

A continuum image was created using the CASA task tclean by considering only the line-free channels within the data. This resulted in a total bandwidth of 6.9 GHz after removing 0.6 GHz around the [C II] emission line. For all of the imaging, we used Briggs weighting with a robust factor of 0.5. To reduce imaging artifacts caused by the sparser sampling at longer baselines, we also applied a *uv*-taper corresponding to a Gaussian with a standard deviation in the image plane of $0\farcs04$. This results in a continuum image with an rms noise level of 4.1 μJy beam^{-1} and a synthesized beam size of $0\farcs076 \times 0\farcs062$ (corresponding to 0.44×0.36 kpc at the redshift of P352–15).

To create the spectral cube, we first subtracted the underlying dust continuum using the task uvcontsub by fitting a zeroth-order polynomial to the line-free channels in the spectral window containing the redshifted [C II] emission line. The spectral cube was then created within *tclean* with channel widths of 31.25 MHz ($\sim$34 km s^{-1}) resulting in an average rms noise of 62 μJy beam^{-1} per channel and a synthesized beam of $0\farcs076 \times 0\farcs063$. We also generated an integrated [C II] map by imaging a single 600 km s^{-1} channel centered on the [C II] emission line (i.e., centered at 278.2976 GHz). This velocity range covers the full [C II] emission of P352–15 ($\Delta V_{\rm FWHM} = 435 \pm 82$ km s^{-1}; S. Rojas-Ruiz et al. 2021). The rms noise of this [C II] map is 19.6 μJy beam^{-1} or 11.8 mJy km s^{-1} beam^{-1} and has the same synthesized beam as the spectral cube. We note that our imaging data have a maximum recoverable scale of $0\farcs6$, implying that our data are not sensitive to emission on larger scales.

3. Results

3.1. ALMA Continuum Emission

The left panel of Figure 1 shows the ALMA continuum map. With an rms noise of 4.1 μJy beam^{-1}, individual emission peaks with a significance of 3σ and higher are located along a linear structure over $0\farcs93$ (5.4 kpc). The peak emission is 37 ± 4 μJy beam^{-1}, corresponding to 9σ. Summing up all emission along the linear feature gives a total flux density of 0.17 mJy, or about 50 % of the flux reported in the lower-resolution (arcsec-scale) imaging presented by S. Rojas-Ruiz et al. (2021).[12] This implies that about half of the continuum emission is not recovered in our highest-resolution observations and is distributed on larger spatial scales, presumably in the host galaxy. It should be stressed that no other of the half-dozen $z \sim 6$ quasars observed at similar subkiloparsec spatial resolution show such a linear clumpy dust continuum structure (e.g., B. P. Venemans et al. 2019; F. Walter et al. 2022; R. A. Meyer et al. 2023; M. Neeleman et al. 2023; R. A. Meyer et al. 2025).

Averaged over the synthesized beam of $\Theta = 0.065''$, $\lambda = 0.107$ cm (corresponding to 278.25 GHz), and using Equation (2.33) in J. J. Condon & S. M. Ransom (2016) and correcting for redshift, this central peak corresponds to a beam-averaged surface brightness temperature contrast of $T_B = 1.1$ K above the extended cosmic microwave background, and the other peaks along the linear structure consequently have even lower surface brightness temperatures. This low temperature implies that the emission is beam-diluted thermal dust emission and not due to nonthermal synchrotron emission. The latter

[12] We note that we recover the same total flux in our data when tapering the emission to a $0\farcs3$ beam.

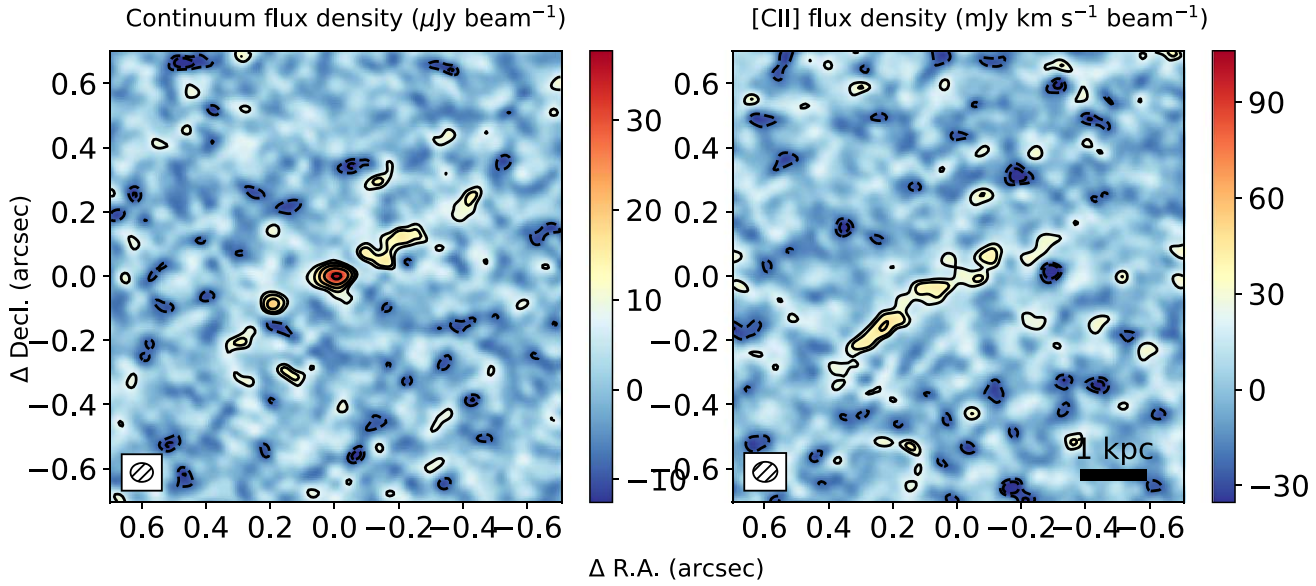

Figure 1. ALMA 400 pc resolution imaging of the dust continuum emission at 285 GHz (left) and the [C II] emission averaged over the central 600 km s^{-1} (right). Contours start at $\pm 2\sigma$ and increase/decrease in powers of $\sqrt{2}$. For the continuum, $1\,\sigma$ corresponds to 4.1 μJy beam^{-1}, and for the [C II] line, $1\sigma = 11.8$ mJy km s^{-1} beam^{-1}. Coordinates are given relative to the brightest source seen in the VLBA observations discussed in Section 3.3 at R.A.(International Celestial Reference System, ICRS) = $23^{\rm h}29^{\rm m}36\overset{\rm s}{.}8316$, decl.(ICRS)= $-15°20'14\overset{''}{.}498$ (E. Momjian et al. 2018). The beam size is indicated in the lower-left corner of both panels, and a 1 kpc scale is shown in the bottom right of the [C II] map.

would have an intrinsic temperature of millions of kelvin, as is the case for the VLBA) synchrotron radio-emitting jet components (E. Momjian et al. 2018). A thermal emission scenario is also in agreement with the radio–FIR spectral energy analysis presented in S. Rojas-Ruiz et al. (2021), which showed that the ALMA continuum emission is mainly (>90%) of thermal origin. Assuming a typical intrinsic temperature of quasar host galaxies of ∼50 K (e.g., C. Leipski et al. 2014) implies that the emission is still significantly clumped within our 400 pc synthesized beam (as seen in the case of the $z = 6.6$ quasar J0305–3150; R. A. Meyer et al. 2025).

If we assume that the dust continuum is indeed powered by star formation, we can derive the corresponding star formation rates (SFRs): using standard assumptions, our 1σ rms noise of 4.2 μJy beam^{-1} corresponds to a total infrared (TIR) luminosity of $L_{\rm TIR} = 1.5 \times 10^{10} L_\odot$ or a TIR-derived 1σ SFR of $1.4\,M_\odot\,{\rm yr}^{-1}$ (R. C. Kennicutt & N. J. Evans 2012), i.e., the individual clumps seen in the ALMA continuum map have implied SFRs in the range of 5–10 $M_\odot\,{\rm yr}^{-1}$, with a central peak SFR of $\sim 13\,M_\odot\,{\rm yr}^{-1}$. For reference, the total TIR-based SFR in P352–15 is $110.0 \pm 13.0\,M_\odot\,{\rm yr}^{-1}$ (S. Rojas-Ruiz et al. 2021).

3.2. Integrated ALMA [C II] Emission

The integrated [C II] map is shown in the right panel of Figure 1. We measure a total [C II] line flux of 0.37 Jy km s^{-1}, or about one third of the total flux reported in S. Rojas-Ruiz et al. (2021). This implies that about two thirds of the [C II] line is distributed over larger scales in the host galaxy (a slightly larger fraction than in the case of the continuum; Section 3.1). This [C II] map shows the same linear structure as the continuum map, albeit over a slightly smaller total extent ($0\overset{''}{.}7$, 4.1 kpc). It is also less symmetric than the dust continuum emission, with excess [C II] emission toward the south–east, compared to the north–west (albeit the respective signal-to-noise ratio (S/N) is not high enough to formally rule out that the emission peaks are different). We discuss the [C II] kinematics in Section 3.5.

3.3. VLBA Observations

VLBA 1.54 GHz observations of the radio jet were reported in E. Momjian et al. (2018), where two possible scenarios are discussed: (i) a radio core with a one-sided jet and (ii) a double-lobed symmetric object. Follow-up VLBA observations at other frequencies now greatly favor scenario (i), where the brightest VLBI source is indeed the core of the system (E. Momjian et al. 2025, in preparation). This implies that the radio counterjet is invisible due to relativistic deboosting effects.

We overplot the VLBA 1.54 GHz image on top of our ALMA observations in Figure 2. For this, we shifted the ALMA images by 24 mas to the west and 5 mas to the north (less than half a synthesized ALMA beam) to align the bright central source in both the ALMA and the VLBA maps. This is justified, as the ALMA astrometry is challenging at these resolutions: according the ALMA Technical Handbook,[13] at resolutions of ∼50 mas the astrometric accuracy is about ∼10% of the synthesized beam if the science target is detected at S/N > 20. In our case, the astrometric accuracy is therefore signal-to-noise limited. As the current observations already represent a 30 hr investment with ALMA, it will be difficult to significantly increase the current signal to noise in the continuum before the completion of the ALMA Wideband Sensitivity Upgrade. For reference, the VLBA observations employed nodding-style phase referencing using the nearby calibrator J2327–1447, with a reported uncertainty in the position of the phase calibrator of 0.09 mas in R.A. and 0.13 mas in decl. (E. Momjian et al. 2018). Within the uncertainties, the positions of the optical quasar and the

[13] Chapter 10 in https://almascience.eso.org/documents-and-tools/cycle8/alma-technical-handbook.

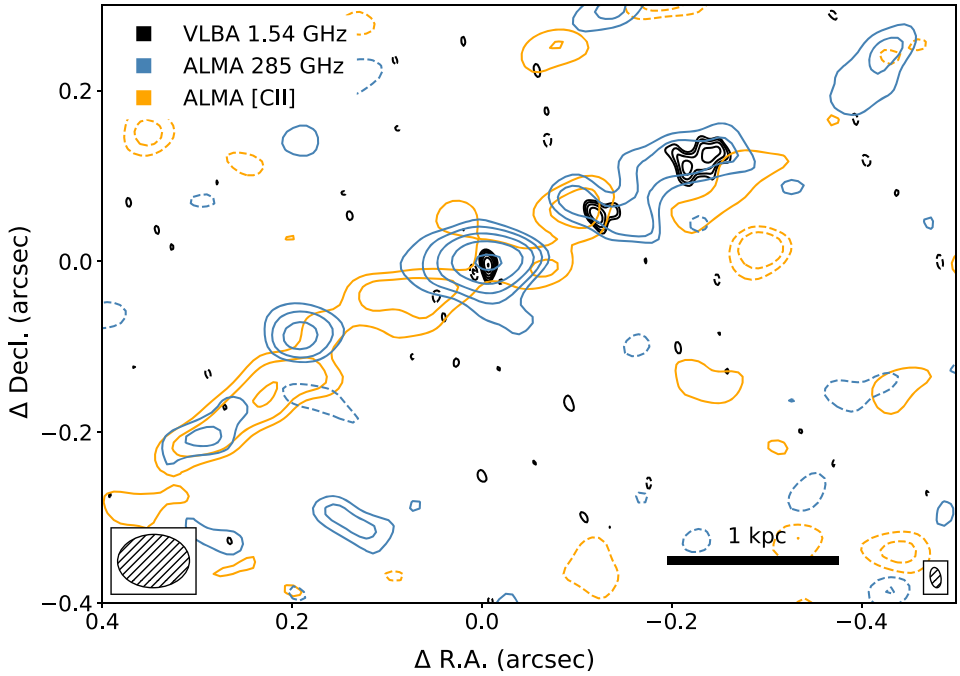

Figure 2. Superposition of the ALMA dust continuum (blue contours), ALMA [C II] emission (orange contours), and the VLBA 1.54 GHz radio continuum image (black contours). The dust continuum emission at 285 GHz and [C II] emission have the same contour levels, as shown in Figure 1. The VLBA image presented in E. Momjian et al. (2018) is shown in black contours starting at $\pm 3\sigma$ ($1\sigma = 67$ μJy beam^{-1}) and increase/decrease by powers of $\sqrt{2}$. The ALMA (VLBA) beam size is indicated in the lower-left (right) corner. The origin in this figure and the kiloparsec-scale bar are as in Figure 1. As discussed in Section 3.3, we have shifted the ALMA data slightly (<25 mas) in order to center the ALMA dust continuum peak on the peak of the VLBA image.

brightest ALMA and VLBA continuum source are thus in agreement.

3.4. Morphology Comparison

When overplotting all three maps (ALMA submillimeter dust continuum, [C II] line emission, and VLBA 1.54 GHz radio continuum emission) in Figure 2, we find clear overall alignment between all structures in P352–15 along the linear structure defined by the VLBA radio jet. We stress that we see [C II] and dust continuum emission associated with the eastern counterjet, which is unseen in radio observations. This makes physical sense: the actual jet is powered on both sides of the central quasar, but only one side is seen in the radio VLBA observations. This is because the relativistic boosting of the side of the jet pointed toward us is contrasted by a deboosting on the opposite side, quenching observed flux. However, if the jet gives rise to enhanced dust (and gas) emission toward both sides (as argued in Section 4), then this enhanced emission will be observed toward both sides in submillimeter emission, as no relativistic effects are at play that would boost or deboost that emission.

The fact that the dust continuum and [C II] emission maxima along the jet do not show strong correspondence presumably implies that the jet encounters different physical conditions as it travels through the interstellar medium of the galaxy. We however note that there is some morphological correspondence between the jet seen in radio and dust continuum. In addition, the ALMA dust continuum image shows some symmetry in the jet and counterjet: the three clumps on either side of the central source are spaced relatively symmetric and might indicate that the quasar activity is bursty in nature. If there were an older episode of a double radio jet, a low-frequency observation might reveal a symmetric large-scale structure in the source (e.g., G. Miley & C. De Breuck 2008).

3.5. Kinematics

In the top-left panel of Figure 3, we show a position–velocity diagram of the [C II] emission along the linear jet structure, centered on the ALMA continuum emission peak. In the top-right panel of the same figure, we show the [C II] velocity field of P352–15 (here the dashed line indicates the orientation of the position–velocity diagram shown in the left). To create this velocity field, we have fitted Gaussian profiles to all pixels detected at $>3\sigma$ in the velocity-integrated flux density map. This approach yields more reliable results in cases of low S/N compared to a first moment image (see, e.g., Appendix C in M. Neeleman et al. 2021). A clear [C II] velocity gradient is apparent; velocities increase approximately linearly as a function of distance from the center, from the systemic velocity of the source to ± 200 km s^{-1}. In creating these maps, we have revised the systemic velocity (and thus redshift) of P352–15 slightly, by ~ -100 km s^{-1}, from $z = 5.831$ to $z = 5.8270$. This shift centers the [C II] spectrum at the nominal position of the quasar (i.e., the point where the continuum emission is maximum). This shift is necessary because significant [C II] emission arises from the jet, which shifts the centroid in the low-resolution data presented in S. Rojas-Ruiz et al. (2021).

From the [C II] kinematics we can reach a number of important conclusions: most importantly, the [C II] velocities encountered are typical for galaxy kinematics and interactions (up to a few 100 km s^{-1}), and we do not find major velocity discontinuities at the level of thousands of km s^{-1}, which might be expected for jet–cloud interactions. (Section 3.4). Second, toward the center (indicated by the black cross and the spectrum at position (B)), there is evidence for enhanced

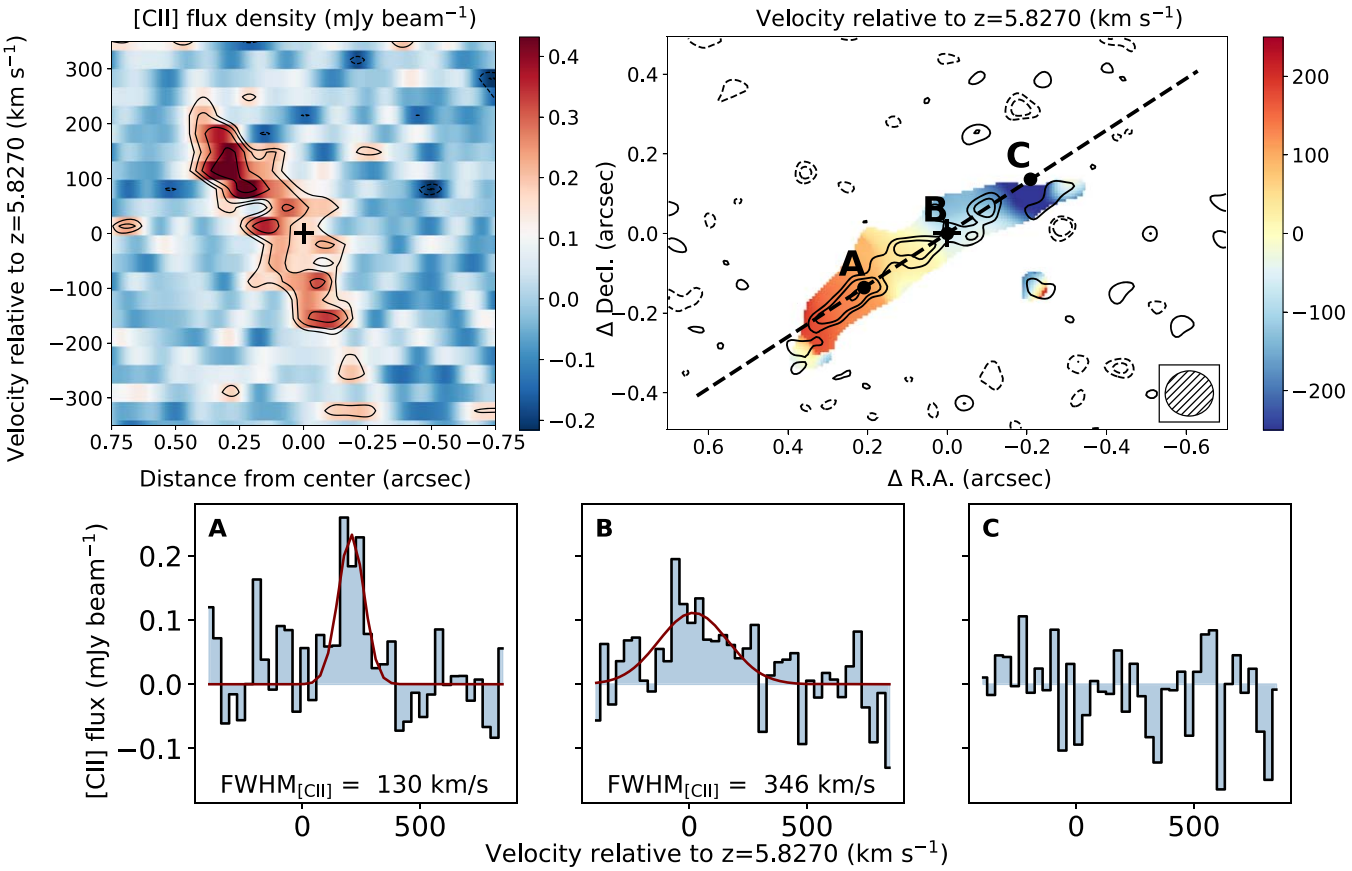

Figure 3. Position–velocity diagram (top left) of the [C II] emission oriented along the direction of the jet as shown by the dashed line (PA = 303°) in the velocity field of the [C II] emission line (top right). In both panels, positive spatial offsets correspond to offsets toward the east. The cross indicates the position of the brightest peak in the VLBA observations (E. Momjian et al. 2018). Contours are plotted in powers of $\sqrt{2}$, starting at $\pm 2\sigma$ (negative contours are dashed). To increase the S/N of the extended emission, we smoothed the data to a resolution of ∼0.″1, as shown by the updated beam in the bottom-right inset of the right panel (the contours in the right panel are the integrated [C II] flux density map using the original resolution shown in Figures 1 and 2). A smooth, linear increase velocity gradient is apparent, reaching maximum velocities of approximately +(−) 200 km s^{-1} along the eastern (western) jet. The bottom panels are single-beam spectra extracted from different positions along the jet (labeled (A), (B), and (C) in top-right panel) spaced 0.″25 apart. The velocity dispersion determined from a Gaussian fit to the data (red line) is given in the two bottom-left panels. No successful fit was obtained for the spectrum at position (C).

velocity dispersion, albeit at low signal to noise. Toward the south (position A), [C II] emission shows a velocity dispersion with a [C II] FWHM of 130 km s^{-1}, consistent with previous dispersion measurements in other $z \gtrsim 6$ quasars based on similarly high-resolution ALMA data (B. P. Venemans et al. 2019; F. Walter et al. 2022; R. A. Meyer et al. 2023, 2025; M. Neeleman et al. 2023).

4. Discussion and Summary

We report 400 pc resolution ALMA imaging of the [C II] line and the 285 GHz dust continuum in P352–15 at $z = 5.83$, a radio-loud quasar at the end of cosmic reionization. The ALMA and VLBA observations reveal a remarkably narrow and linear correlation between the [C II], thermal dust, and VLBA radio synchrotron emission, with a full length of about 4 kpc and width at least 10 times smaller. The gas kinematics show a simple linear velocity gradient, with velocities that are consistent with those encountered in typical galactic environments.

We interpret our findings with the following physical picture: Consider a galaxy-wide distribution of cool gas and dust in the quasar host galaxy with a large-scale velocity gradient due to rotation, galaxy interactions, or infall of gas. However, this emission on galactic scales is too faint to be mapped out with our current 400 pc resolution data. A powerful relativistic radio jet is launched by the central quasar and rapidly passes through the host galaxy and its interstellar medium. Synchrotron emission is seen from radio jet knots, which form and fade on short timescales in regions of enhanced jet–cloud interaction (on timescales of thousands of years or even less; e.g., M. Perucho et al. 2014). In these same regions, shocks driven by the jet compress the local clouds, heat the interstellar medium, and may even induce some clouds to form stars ("positive feedback"). In turn, this injection of turbulent energy (and possibly star formation) heats the dust, giving rise to the observed rest-frame FIR continuum and [C II] line emission seen by ALMA. The passage of the jet thus effectively leaves a "streak" of enhanced thermal dust continuum and [C II] emission, which would be persistent on timescales longer than its cause (the radio jet with relativistic speeds). If this emission was associated with star formation, it would likely even persist for much longer (millions of years) than most of the radio continuum jet emission. The fact that we do not see any "streaks" of enhanced star formation in radio-quiet quasars (assuming they were radio loud at some point in their past) would then suggest that either the timescales for this enhanced star formation are comparable to the timescales of the jet or otherwise dynamical processes within the disk (e,g.,

mergers and disk rotation) quickly remove any evidence of jet-triggered enhanced star formation.

This situation resembles the well-studied radio-optical "alignment effect" in high-redshift radio galaxies, in which a general alignment is seen between the kiloparsec-scale radio jet direction and the optical starlight and Lyα emission on scales out to tens of kiloparsecs (e.g., P. J. McCarthy et al. 1990). In most cases, this alignment is not exact but is seen as just a broad agreement. However, there is at least one case, the $z = 3.8$ radio galaxy 4C 41.17, where the alignment between starlight, Lyα, [C I] and CO emission, and the radio jet is remarkably close, linear, and narrow in the inner jet on a scale of $\sim$14 kpc (G. V. Bicknell et al. 2000; N. P. H. Nesvadba et al. 2020), similar to what is seen in P352–15. In 4C 41.17 these authors argue, from the close correlation between bright radio knots with optical components, as well as from the broad velocity dispersions of the C IV and millimeter emission lines, for jet-induced star formation, where shocks caused by the advancing radio source compress the dense clouds and enhance star formation on a timescale of order 10^6 yr. Thus, 4C 41.17 perhaps shows the most direct evidence for positive "radio-mode feedback" in a distant galaxy, where the expanding radio source enhances the galaxy formation process through induced star formation. An alternative physical interpretation for the alignment effect was introduced by S. A. Eales (1992). In this interpretation, radio hotspots are brightened when they travel through a high-density environment.

Our high-resolution ALMA imaging of P352–15 shows a similar, very close alignment of the axes of multiple components (in our case gas and dust) of the host galaxy with the radio jet. The [C II] velocity dispersion along the jet in P352–15 is significant ($\gtrsim$100 km s^{-1}), hinting at kinematic evidence for jet–cloud interactions. However, there are differences between P352–15 and 4C 41.17, principally relating to the fact that P352–15 is a broad-line radio-loud quasar (E. Bañados et al. 2018), not a radio galaxy: a Very Large Telescope X-shooter optical near-infrared spectrum shows a typical high-redshift quasar spectrum, including broad Lyα that is truncated at short wavelength due to Lyα resonant scattering by a significantly neutral intergalactic medium, as well as broad C IV emission with a line width of 4330 km s^{-1}, from which a black hole mass of $\sim 10^9\ M_\odot$ has been derived (Z. L. Xie et al. 2025, in preparation). Further, Chandra observations show that P352–15 has an X-ray power-law spectrum and optical to X-ray luminosity ratio characteristic of high-redshift quasars (T. Connor et al. 2021).

Potentially counter to the above scenario is a recent study of the integrated radio spectrum of P352–15, which shows a clear steepening in the spectrum around an observed frequency of 30 GHz out to 100 GHz (S. Rojas-Ruiz et al. 2025), from which they derive a synchrotron/inverse Compton "spectral age" for the radio source of order 500 yr, depending on the magnetic field strength. This is very short compared to the timescale that would be required for jet-induced star formation to proceed (millions of years). Alternatively, the jet activity could be episodic, with previous episodes giving rise to the emission seen in the ALMA observations. In any case, the astonishingly close alignment and narrow linearity of the radio jet with the [C II] and dust emission are hard to conceive without some fundamental relationship between the two. Reconciling the respective timescales remains paramount to understanding the nature of P352–15.

Acknowledgments

We thank Santiago Garcia-Burillo, Ryan Keenan, and Alessandro Lupi for useful discussions. This Letter makes use of the following ALMA data: ADS/JAO.ALMA#2018.1.00656.S and 2022.1.01587.S. ALMA is a partnership of ESO (representing its member states), NSF (USA), and NINS (Japan), together with NRC (Canada), MOST and ASIAA (Taiwan), and KASI (Republic of Korea), in cooperation with the Republic of Chile. The Joint ALMA Observatory is operated by ESO, AUI/NRAO, and NAOJ. The National Radio Astronomy Observatory is a facility of the National Science Foundation operated under cooperative agreement by Associated Universities, Inc. C.M. acknowledges support from Fondecyt Iniciacion grant 11240336 and the ANID BASAL project FB210003. R.A.M., M.N., and F. W. acknowledge support from the ERC Advanced grant 740246 (Cosmic_Gas). R.A.M. acknowledges support from the Swiss National Science Foundation (SNSF) through project grant 200020_207349.

Facilities: ALMA

Software: Astropy (Astropy Collaboration et al. 2018), CASA (J. P. McMullin et al. 2007), Matplotlib (J. D. Hunter 2007, http://www.matplotlib.org).

ORCID iDs

Fabian Walter https://orcid.org/0000-0003-4793-7880
Eduardo Bañados https://orcid.org/0000-0002-2931-7824
Chris Carilli https://orcid.org/0000-0001-6647-3861
Marcel Neeleman https://orcid.org/0000-0002-9838-8191
Thomas Connor https://orcid.org/0000-0002-7898-7664
Roberto Decarli https://orcid.org/0000-0002-2662-8803
Emanuele Paulo Farina https://orcid.org/0000-0002-6822-2254
Yana Khusanova https://orcid.org/0000-0002-7220-397X
Chiara Mazzucchelli https://orcid.org/0000-0002-5941-5214
Romain Meyer https://orcid.org/0000-0001-5492-4522
Emmanuel Momjian https://orcid.org/0000-0003-3168-5922
Hans–Walter Rix https://orcid.org/0000-0003-4996-9069
Sofía Rojas-Ruiz https://orcid.org/0000-0003-2349-9310
Bram Venemans https://orcid.org/0000-0001-9024-8322

References

Astropy Collaboration, Price-Whelan, A. M., Sipőcz, B. M., et al. 2018, AJ, 156, 123
Bañados, E., Carilli, C., Walter, F., et al. 2018, ApJL, 861, L14
Bertoldi, F., Cox, P., Neri, R., et al. 2003, A&A, 409, L47
Bicknell, G. V., Sutherland, R. S., van Breugel, W. J. M., et al. 2000, ApJ, 540, 678
CASA Team, Bean, B., Bhatnagar, S., et al. 2022, PASP, 134, 114501
Condon, J. J., & Ransom, S. M. 2016, Essential Radio Astronomy (Princeton, NJ: Princeton Univ. Press)
Connor, T., Bañados, E., Stern, D., et al. 2021, ApJ, 911, 120
Decarli, R., Loiacono, F., Farina, E. P., et al. 2024, A&A, 689, A219
Decarli, R., Walter, F., Venemans, B. P., et al. 2018, ApJ, 854, 97
Ding, X., Onoue, M., Silverman, J. D., et al. 2023, Natur, 621, 51
Eales, S. A. 1992, ApJ, 397, 49
Fabian, A. C. 2012, ARA&A, 50, 455
Fan, X., Bañados, E., & Simcoe, R. A. 2023, ARA&A, 61, 373
Fan, X., Narayanan, V. K., Lupton, R. H., et al. 2001, AJ, 122, 2833
Habouzit, M., Li, Y., Somerville, R. S., et al. 2021, MNRAS, 503, 1940
Hunter, J. D. 2007, CSE, 9, 90
Hunter, T. R., Indebetouw, R., Brogan, C. L., et al. 2023, PASP, 135, 074501
Kennicutt, R. C., & Evans, N. J. 2012, ARA&A, 50, 531
Leipski, C., Meisenheimer, K., Walter, F., et al. 2014, ApJ, 785, 154
Mahieu, S., Maier, D., Lazareff, B., et al. 2012, ITTST, 2, 29
Maiolino, R., Cox, P., Caselli, P., et al. 2005, A&A, 440, L51

McCarthy, P. J., Spinrad, H., van Breugel, W., et al. 1990, ApJ, 365, 487
McMullin, J. P., Waters, B., Schiebel, D., Young, W., & Golap, K. 2007, in ASP Conf. Ser. 376, Astronomical Data Analysis Software and Systems XVI, ed. R. A. Shaw, F. Hill, & D. J. Bell (San Francisco, CA: ASP), 127
Meyer, R. A., Neeleman, M., Walter, F., & Venemans, B. 2023, ApJ, 956, 127
Meyer, R. A., Venemans, B., Neeleman, M., Decarli, R., & Walter, F. 2025, ApJ, 980, 20
Miley, G., & De Breuck, C. 2008, A&ARv, 15, 67
Momjian, E., Carilli, C. L., Bañados, E., Walter, F., & Venemans, B. P. 2018, ApJ, 861, 86
Neeleman, M., Novak, M., Venemans, B. P., et al. 2021, ApJ, 911, 141
Neeleman, M., Walter, F., Decarli, R., et al. 2023, ApJ, 958, 132
Nesvadba, N. P. H., Bicknell, G. V., Mukherjee, D., & Wagner, A. Y. 2020, A&A, 639, L13
Nesvadba, N. P. H., De Breuck, C., Lehnert, M. D., Best, P. N., & Collet, C. 2017, A&A, 599, A123
Onoue, M., Ding, X., Silverman, J. D., et al. 2024, arXiv:2409.07113
Perucho, M., Martí, J.-M., Quilis, V., & Ricciardelli, E. 2014, MNRAS, 445, 1462
Rojas-Ruiz, S., Bañados, E., Neeleman, M., et al. 2021, ApJ, 920, 150
Rojas-Ruiz, S., Momjian, E., Davies, F. B., et al. 2025, arXiv:2503.16609
Russell, H. R., McNamara, B. R., Edge, A. C., et al. 2013, MNRAS, 432, 530
Venemans, B. P., Decarli, R., Walter, F., et al. 2018, ApJ, 866, 159
Venemans, B. P., Neeleman, M., Walter, F., et al. 2019, ApJL, 874, L30
Volonteri, M., Habouzit, M., & Colpi, M. 2021, NatRP, 3, 732
Walter, F., Bertoldi, F., Carilli, C., et al. 2003, Natur, 424, 406
Walter, F., Carilli, C., Bertoldi, F., et al. 2004, ApJL, 615, L17
Walter, F., Neeleman, M., Decarli, R., et al. 2022, ApJ, 927, 21
Wylezalek, D., & Morganti, R. 2018, NatAs, 2, 181